Effects of Single-Walled Carbon Nanotubes on the Crystallization Behavior of Polypropylene

L. Valentini,[1] J. Biagiotti,[1] J. M. Kenny,[1] S. Santucci[2]

[1] *Materials Engineering Center, Università di Perugia, 05100 Terni, Italy*
[2] *Dipartimento di Fisica, Unità INFM, Università dell'Aquila, 67010 Coppito (AQ), Italy*

Received 25 February 2002; accepted 26 April 2002

ABSTRACT: Polypropylene matrix composites reinforced with single-walled carbon nanotubes (SWNTs) were produced with different nanotube concentrations. The characterization of these new materials was performed by differential scanning calorimetry and Raman and Fourier transform infrared spectroscopy to obtain information on the matrix–nanotube interaction, on the crystallization kinetics of polypropylene, and especially on the macrostructure and organization of the nanotubes in the composite. On the one hand, the results confirmed the expected nucleant effect of nanotubes on the crystallization of polypropylene, but on the other hand, this effect was not linearly dependent on the SWNT content: there was a saturation of the nucleant effect at low nanotube concentrations. Raman spectroscopy was successfully applied to demonstrating that in the composite films, the crystallization kinetics were strongly affected by the distance between the nanotube bundles as a result of a different intercalation of the polymer. J Appl Polym Sci 87: 708–713, 2003

Key words: nanocomposites; poly(propylene) (PP); differential scanning calorimetry (DSC); Raman spectroscopy

INTRODUCTION

Because of the unusual mechanical[1,2] and electronic properties,[3,4] extensive studies have been devoted to the use of carbon nanotubes (CNTs) as nanofibers to improve the performance of a matrix or to achieve new properties.[5–8] One of the advantages of CNTs as reinforcements is their large surface area, which can induce better adhesion with the polymeric matrix, which is an important factor for an effective enhancement of the composite properties.[9,10]

Among the most versatile polymer matrices, polyolefins such as polypropylene (PP) are the thermoplastics of higher consumption because of their well-balanced physical and mechanical properties and their easy processability at a relatively low cost. In PP matrix composites, the crystalline morphology of the polymer can be influenced by the fibers, which can act as nucleant agents influencing the crystallization process. Recent developments of nanofiller-reinforced composites have shown that it is possible to obtain well-performing materials.[11] To unlock the potential of CNTs for applications in thermoplastic matrix-based nanofiller composites, we need to analyze the crystallization behavior and the consequent microstructure of such polymers to provide useful information for the design of processing operations.

Correspondence to: J. M. Kenny (kenny@unipg.it).

Journal of Applied Polymer Science, Vol. 87, 708–713 (2003)

In this work, we investigated the effects of different concentrations of single-walled carbon nanotubes (SWNTs) on the crystalline kinetics and morphology of PP matrix composites. The thermal characterization was performed with differential scanning calorimetry (DSC). The vibrational properties of the composites at several nanotube concentrations were studied with Raman spectroscopy. Fourier transform infrared (FTIR) spectroscopy was then used to examine the possible chemical interactions between the two materials.

EXPERIMENTAL

A commercially available grade of isotactic polypropylene (iPP; melt-flow index = 2.9 dg/min at 190°C and 5 kg, density = 0.90 g/cm^3), kindly supplied by Solvay (Brussels, Belgium) under the trade name of Eltex-P HV-200, was used in this work. Nanotubes (SWNTs) were commercially obtained from CarboLex (Kentucky). The material consists of packed bundles of nanotubes with individual diameters equal to 12–20 Å. There are about 30 nanotubes per bundle (with an average bundle diameter of 100 Å) with a length of several micrometers.

For the composite production, PP was melt-blended with the addition of several nanotube concentrations specified as weight percentages in the polymer: 5, 10, 15, and 20%. The temperature of the mixing system was estimated by a thermocouple regulation to 190°C, and the blending time was 10 min.

The nonisothermal thermal analysis was performed with a PerkinElmer (Maryland) Pyris 1 differential

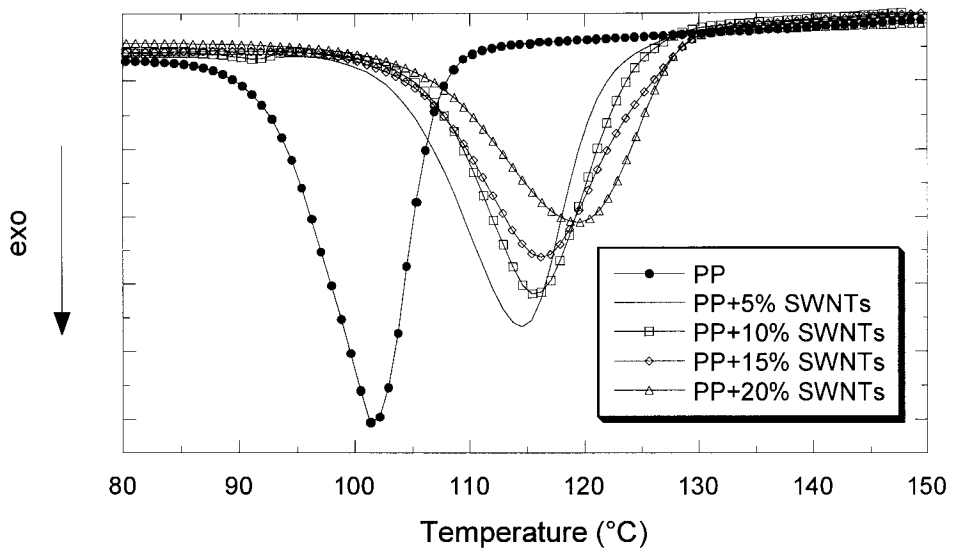

Figure 1 Nonisothermal crystallization curves of PP and PP-SWNT composites.

scanning calorimeter coupled to an intercooler. The standard procedure performed in the scans was as follows: Samples of about 8 mg were heated from 30 to 200°C at a scan rate of 10°C/min and held there for 10 min to eliminate any thermal history of the material. Subsequently, the samples were cooled to −50°C with scan rates of 50°C/min. For the observation of the melting peak after crystallization, the samples were then heated to 200°C.

The crystalline morphology of the samples was studied on films with an optical polarizing microscope (Hund Weztlar H600) equipped with a Mettler FP-82 HT automatic hot-stage thermal control. Samples were melted and squeezed between microscope cover glasses at 200°C for 10 min and then rapidly cooled to the isothermal crystallization temperature of 130°C.

Raman scattering spectra were recorded with a Jobin Yvon (France) micro-Raman LabRam system in a backscattering geometry. A 632.8-nm (1.96-eV) He–Ne laser was used as the light source, and the power of the laser was adjusted with optical filters. With a 100× objective lens, the illuminated spot on the sample surface was focused to about a 2μm diameter. The resolution of the Raman spectra was better than 1 cm^{-1}. The typical acquisition time for the spectra was 30 s. Finally, IR spectra were recorded with a Jasco (Easton, MD) 615 FTIR spectrometer.

RESULTS

The effects of SWNTs on the crystallization of iPP were analyzed with nonisothermal DSC experiments. Figure 1 shows the dynamic thermograms obtained for neat PP and its composites. The crystallization peak (T_c), the apparent melting temperatures (T_m's) of the crystallized samples, and the crystallization enthalpy (ΔH) as a function of the SWNT concentration are reported in Table I. The observed dynamic crystallization behavior shows the positive effects of the nanotubes on the crystallization kinetics of PP. In particular, Table I values confirm that the addition of SWNTs to the polymer matrix produces an increase in T_c. The relative shift of T_c is quite evident at the lowest reinforcement content with a slow but continuous further increase with the SWNT concentration. These results confirm that the addition of a low concentration of nanotubes enhances the nucleation process for iPP crystallization. The decrease in ΔH with an increasing nanotube concentration can be directly attributed to the proportional reduction of the PP concentration in the composite. Furthermore, no significant changes in the melting point of the PP phase were detected in the blends.

Figure 2 shows microphotographs of the crystalline morphology, at the end of the crystallization process, of samples prepared with 0 and 5% SWNTs. For the neat PP, large grains can be observed (average diameter ~ 100 μm). For the 5% concentration sample, a large quantity of small crystal aggregates are visible (average diameter ~ 10 μm). For higher concentrations, the large presence of nanotube bundles on the

TABLE I
T_c, T_m, and ΔH of PP and PP–SWNT Composites

Material	T_c (°C)	ΔH (J/g)	T_m (°C)
Neat PP	101.31	102.41	166.11
PP + 5% SWNTs	114.56	97.32	163.28
PP + 10% SWNTs	115.41	92.98	163.44
PP + 15% SWNTs	116.21	87.65	164.44
PP + 20% SWNTs	119.61	82.79	165.11

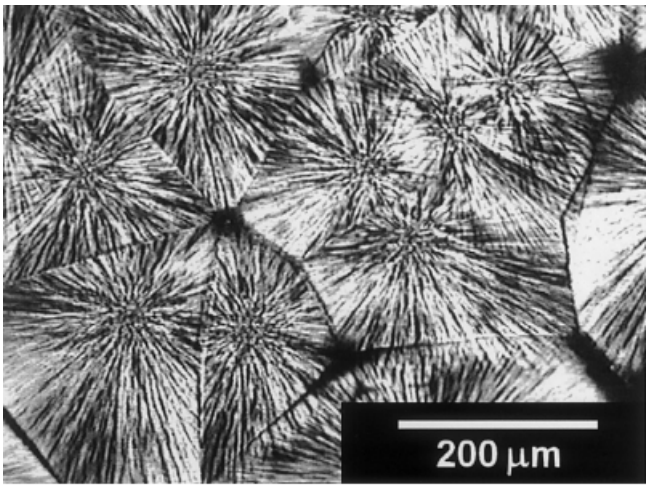

(a)

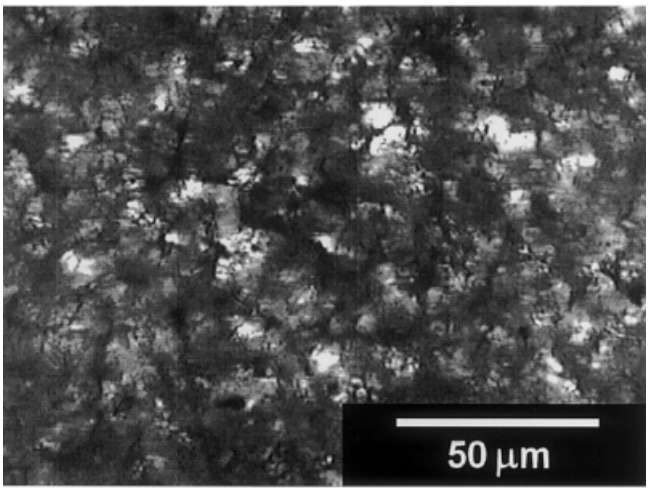

(b)

Figure 2 Microphotographs of (a) neat PP and (b) a 5 wt % SWNT composite.

samples increases the optical absorption, hindering image acquisition.

The high-frequency parts of the Raman spectra of SWNTS and the composites for several nanotube concentrations (5, 10, 15, and 20%) are reported in Figure 3. The Raman bands of SWNTs are clearly observed in the PP-SWNT spectra, but the PP ones do not appear because of their low intensity. The spectra exhibit peaks at 1275, 1549, and 1589 cm^{-1}. The band generally localized around 1275 cm^{-1} is assigned to the D line of graphite and corresponds to the disordered graphite structures.[12–14]

We then analyzed the spectra quantitatively by searching the minimum number of frequencies that fit the different Raman bands without fixing the position and widths of the individual peaks. The area ratio of the shoulders in the high-frequency spectra, that is, the peaks at 1549 and 1589 cm^{-1}, compared with that of the nanotubes is reported in Figure 4(A). The results show an increase in the area ratio with the nanotube concentration increasing up to 15%; for higher concentrations, the increase is reduced. Figure 4(B) shows the dependence of the D-peak position and its width on SWNT incorporation. The main feature of these results is the shift to higher frequencies of the D-peak position accompanied by a reduction of its width with an increasing amount of nanotubes incorporated into the composite.

The Raman spectra recorded for the same samples in the low-frequency part show a well-pronounced peak around 100–200 cm^{-1} (Fig. 5). This band is attributed to the breathing mode A_{1g} of nanotubes, and its frequency depends on the inverse diameter.[15] With the same fitting procedure explained previously, three main features appear in the PP-SWNT spectra at 145, 160, and 200 cm^{-1}. From Figure 6, it is clear that the aforementioned peaks are shifted up when a low concentration of nanotubes is introduced into PP. The shift in the frequency of the feature depends on the nanotube diameter. The lower frequencies, which correspond to the higher diameters, increase more than the higher ones.

A further characterization of the film structure was performed with IR spectroscopy. Typical FTIR absorption spectra in the 2700–3200-cm^{-1} range of both PP and its composites at two concentrations (5 and 20%) are reported in Figure 7. The CH stretch region (2700–3200 cm^{-1}) consists of three peaks:[16] at 2850 cm^{-1} for symmetric sp^3 CH_s, at 2920 cm^{-1} for asymmetric sp^3 CH_2–sp^3 CH, and at 2960 cm^{-1} for asymmetric sp^3 CH_3 stretching modes. As can be seen in Figure 7, the intensities of these modes change with the progressive incorporation of SWNTs.

DISCUSSION

The observed changes in PP crystallization are certainly a result of microstructural changes induced by the incorporation of SWNTs. In particular, in neat

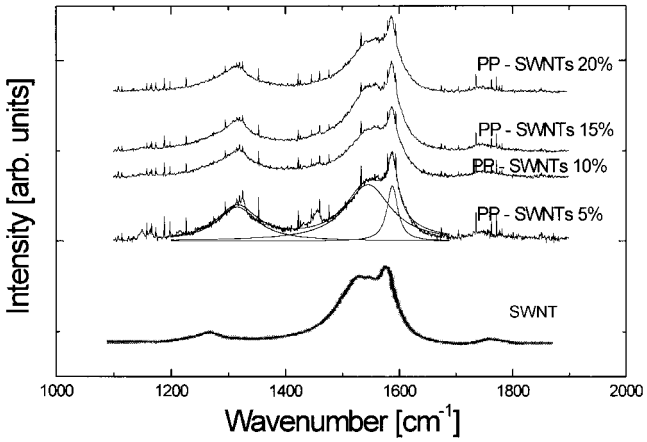

Figure 3 High-frequency Raman spectra of SWNT and PP-SWNT 5% composites.

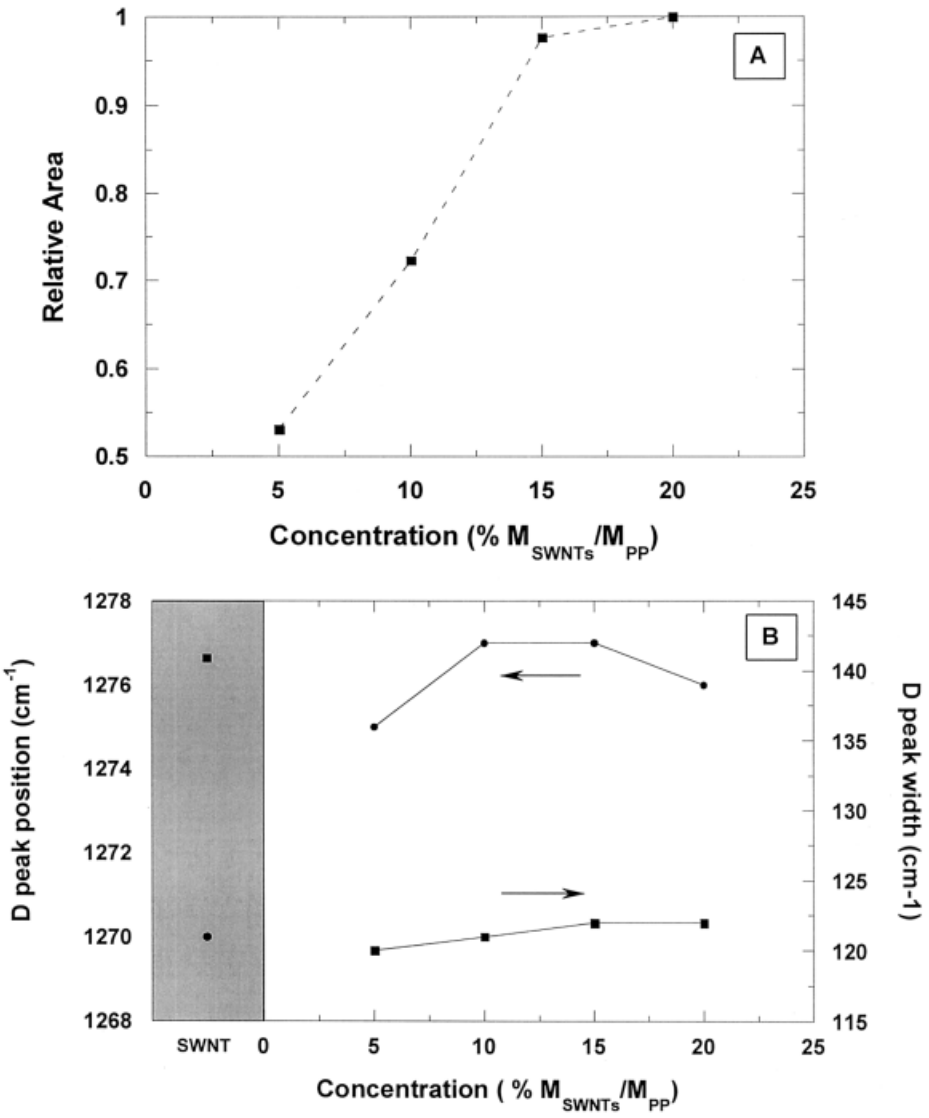

Figure 4 (A) Relative areas of bands at 1549 and 1589 cm^{-1} of the composite spectra compared with those of the nanotubes and (B) D-band positions and D-band widths of SWNT and PP-SWNT composites for several concentrations.

nanotube samples, the band generally localized around 1275 cm^{-1} can be attributed to the defects in nanotubes and to the tube curvature.[17–22] In our case, the peak observed at 1270 cm^{-1} in the SWNT spectra (Fig. 3) has an asymmetric profile on its low-frequency side indicating an additional contribution. In fact, the Raman spectrum of amorphous carbon shows that the so-called D band of amorphous carbon peaks at 1260 cm^{-1} and may constitute the low-frequency part of the 1270-cm^{-1} band observed in the SWNT Raman spectra.[17] With the introduction of nanotubes into PP, the feature at 1270 cm^{-1} is shifted up to 1275 cm^{-1}, and its width is narrower. Then, the peak observed at 1260 cm^{-1} for neat SWNTs decreases in intensity in the composite, indicating a dilution effect of the CNTs when blended with PP. Moreover, each peak from the decomposition of the low-frequency bands can be attributed to the nanotube bundle dimension. When the nanotubes are incorporated into the polymer, they are shifted toward higher frequencies, especially the lower frequency peaks; then, the shifts observed can be explained by the intercalation of the polymer into the bundles. In fact, the polymer exerts a pressure on the individual tubes, increasing the breathing-mode frequencies. Furthermore, in the low-concentration samples, the quantity of PP intercalated between nanotubes could lead to an opening of the bundles, enhancing the formation of nucleant agents to favor the crystallization process.

The shift of the breathing modes can be connected to the modifications observed in the high-frequency bands. The phenomenon can be explained if we consider the composite/nanotube area ratio of the shoulders in the high-frequency spectra, that is, the peaks at 1549 and 1589 cm^{-1}. The observed increase in the area ratio when the nanotube concentration is increased

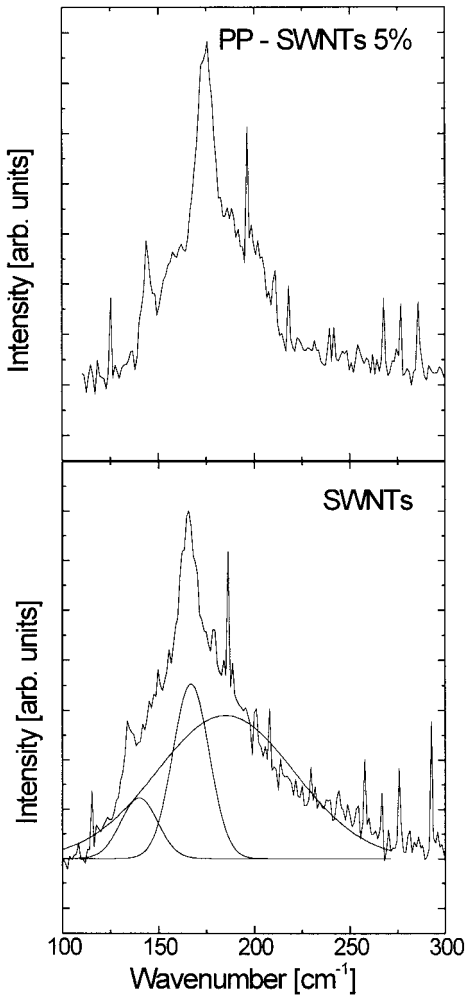

Figure 5 Low-frequency Raman spectra of SWNT and PP-SWNT 5% composites.

from 5 to 15% [Fig. 4(A)] suggests that the quantity of the polymer intercalated between nanotubes decreases; eventually, bundles become stable for concentrations higher than 15%, and this indicates a saturation of the composite. Therefore, the behavior of the features at 1549 and 1589 cm^{-1} shows two extreme situations. For low nanotube concentrations, an intercalation of the polymer between SWNTs in bundles is allowed, leading to an increase in the nanotube dispersion. Therefore, the interactions between nanotubes become very low, and the bundles can be desegregated. At high nanotube concentrations, the structure of the bundles seems unchanged, and the quantity of aggregates increases with the filler concentration; this keeps the polymer away from intercalation.

According to a simulation study performed on polyethylene and CNTs,[23] the intensity increase in the features at 2920 and 2950 cm^{-1} shown by IR spectroscopy reveals the formation of chemical bonds between the polymer matrix and SWNTs. In particular, it is assumed that the high chemical reactivity of CNTs with hydrogen remotion from PP induces the formation of sp^3 bonds with a π orbital on the CNT surface. This could explain the observed reduction of the peak located at 2850 cm^{-1}, which is accompanied by an increase in the intensity of the two features at higher frequencies.

CONCLUSIONS

The effects of different SWNT concentrations on the crystallization of iPP were analyzed by thermal analysis, optical microscopy, and Raman and IR spectroscopy. It has been demonstrated that the incorporation of nanotubes affects the crystalline behavior and struc-

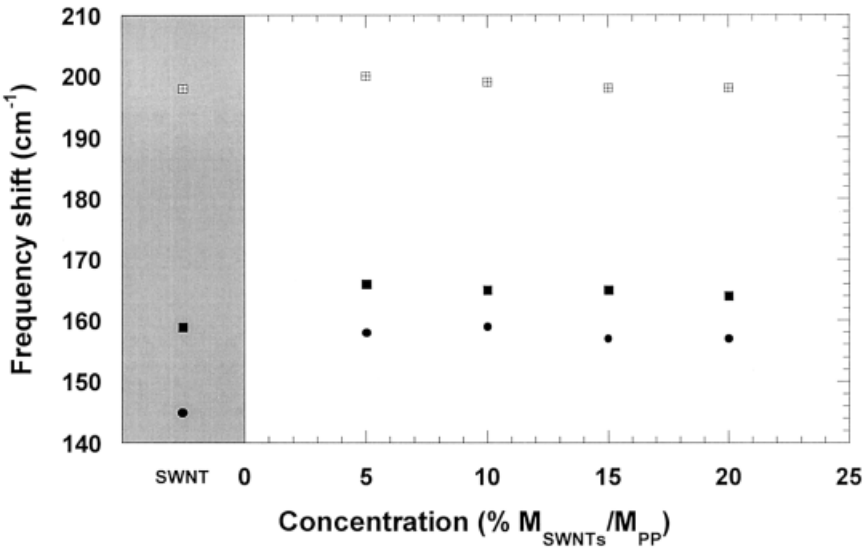

Figure 6 Decomposition of the low-frequency bands of SWNT and PP-SWNT composites for several concentrations. (●) 145 cm^{-1}; (■) 160 cm^{-1}; (⊞) 200 cm^{-1}.

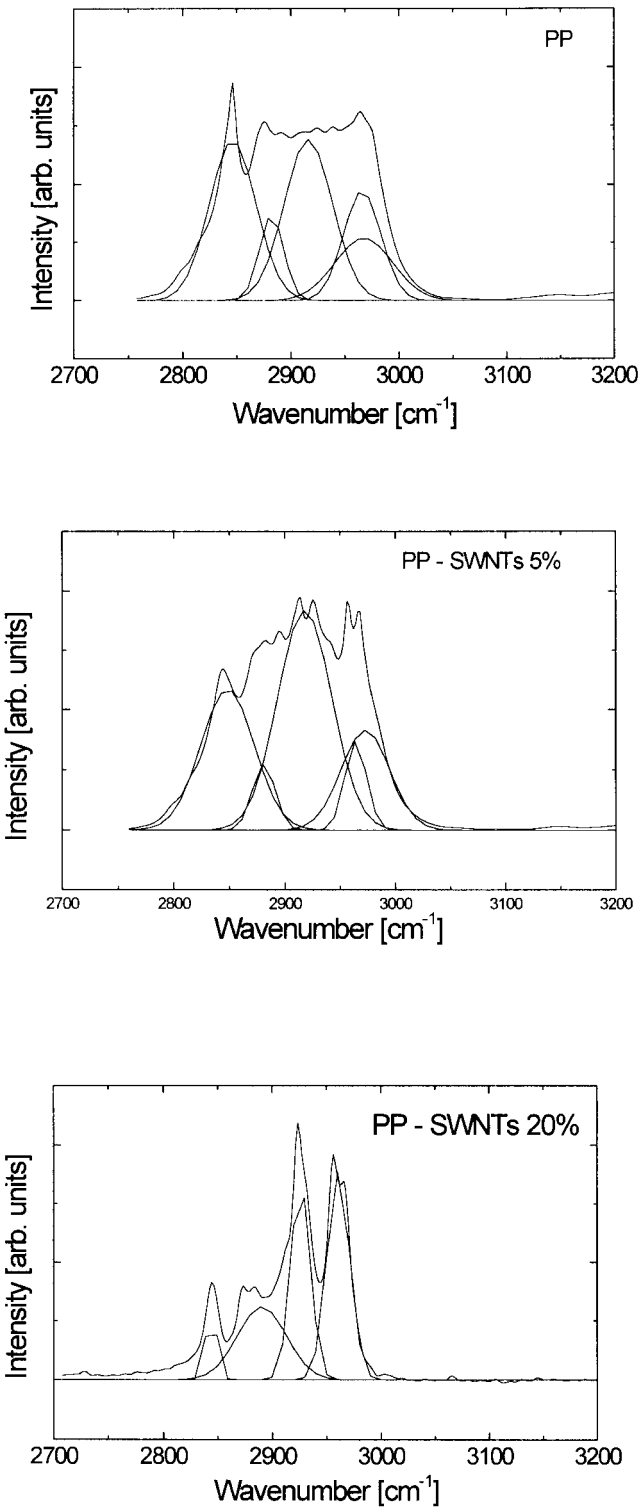

Figure 7 FTIR spectral bands of PP and PP-SWNT composites for 5 and 20% concentrations.

ture of the PP matrix. In particular, SWNTs accelerate the nucleation and crystal growth mechanisms of PP, this effect being more noticeable at the lower filler content analyzed (5%). The crystalline morphology observed by microscopy confirms the thermal analysis results concerning the positive effects of low SWNT concentrations on nucleation and crystallization kinetics. These results find an explanation in terms of the chemical and microstructural changes evidenced by IR and Raman spectroscopy. The changes in the low-frequency Raman bands demonstrate that, for the low nanotube concentration, the polymer is intercalated between nanotubes into bundles that can be desegregated. However, when the nanotube concentration is high, the large quantity of nanotubes does not allow the intercalation of a large quantity of polymer between SWNTs into bundles. The IR spectra performed for PP-SWNTs support the hypothesis that chemical bonding between the polymer and CNTs is energetically favored.

References

1. Treacy, M. M. J.; Ebbensen, T. W.; Giblson, J. M. Nature 1996, 381, 678.
2. Lourie, O.; Cox, D. M.; Wagner, H. D. Phys Rev Lett 1998, 81, 1638.
3. Satio, R.; Fujita, M.; Dresselhaus, G.; Dresselhaus, M. S. Phys Rev B 1992, 46, 1804.
4. Langer, L.; Bayot, V.; Grivei, E.; Issi, J.-P.; Heremans, J. P.; Olk, C. H.; Stockman, L.; Van Haesendonck, C.; Bruynseraede, Y. Phys Rev Lett 1996, 76, 479.
5. Schadler, L. S.; Giannaris, S. C.; Ajayan, P. M. Appl Phys Lett 1998, 73, 3842.
6. Andrews, R.; Jacques, D.; Rao, A. M.; Rantell, T.; Derbyshire, F.; Chen, Y.; Chen, J.; Haddon, R. C. Appl Phys Lett 1999, 75, 1329.
7. Ajayan, P. M.; Schadler, L. S.; Giannaris, C.; Rubio, A. Adv Mater 2000, 12, 750.
8. Qian, D.; Dickey, E. C.; Andrews, R.; Rantell, T. Appl Phys Lett 2000, 76, 2868.
9. Stephan, C.; Nguyen, T. P.; Lamy de la Chepelle, M.; Lefrant, S.; Journet, C.; Bernier, P. Synth Met 2000, 108, 139.
10. Curran, S.; Ajayan, P.; Blau, W.; Carrol, D.; Coleman, J.; Dalton, A.; Davey, A. P.; McCarthy, B.; Stevens, A. Adv Mater 1998, 10, 1091.
11. Alexandre, M.; Dubois, P. Mater Sci Eng 2000, 28, 1.
12. Dresselhaus, M. S.; Eklund, P. C. Adv Phys 2000, 49, 705.
13. Rao, A. M.; Jorio, A.; Pimenta, M. A.; Dantas, M. S.; Saito, R.; Dresselhaus, G.; Dresselhaus, M. S. Phys Rev Lett 2000, 84, 1820.
14. Brown, S. D.; Jorio, A.; Dresselhaus, G.; Dresselhaus, M. S. Phys Rev B 2001, 64, 73403.
15. Bandow, S.; Asaka, Y.; Saito, Rao, A. M.; Grigorian, L.; Richter, E.; Eklund, P. C. Phys Rev Lett 1998, 80, 3779.
16. McNamara, K. M.; Williams, B. E.; Gleason, K. K.; Scruggs, B. E. J Appl Phys 1994, 76, 2466.
17. de la Chappelle, M. L.; Lefrant, S.; Journet, C.; Maser, W.; Bernier, P.; Loiseau, A. Carbon 1998, 36, 705.
18. Eklund, P. C.; Holden, J. M.; Jishi, R. A. Carbon 1995, 33, 959.
19. Rao, A. M.; Richter, E.; Bandow, S.; Chase, B.; Eklund, P. C.; Williams, K. A.; Fang, S.; Subbaswamy, K. R.; Menon, M.; Thess, A.; Smalley, R. E.; Dresselhaus, G.; Dresselhaus, M. S. Science 1997, 275, 187.
20. Rinzler, A. G.; Liu, J.; Dai, H.; Nikolaev, P.; Huffman, C. B.; Rodriguez-Macias, F. J.; Boul, P. J.; Lu, A. H.; Heymann, D.; Colbert, D. T.; Lee, R. S.; Fischer, J. E.; Rao, A. M.; Eklund, P. C.; Smalley, R. E. Appl Phys A 1998, 67, 29.
21. Iliev, M. N.; Litvinchuk, A. P.; Arepalli, S.; Nikolaev, P.; Scott, C. D. Chem Phys Lett 2000, 316, 217.
22. Pimenta, M. A.; Marucci, A.; Brown, S. D. M.; Mattews, M. J.; Rao, A. M.; Eklund, P. C.; Smalley, R. E.; Dresselhaus, G.; Dresselhaus, M. S. J Mater Res 1998, 13, 2396.
23. Wei, C.; Cho, K.; Srivastave, D. MRS Spring Meeting Proc Pap.